

PERFORMANCE OF THE SPIRAL LINE INDUCTION ACCELERATOR

J.R. Smith, V.L. Bailey, H. Lackner, and S.D. Putnam

Pulse Sciences, Inc
San Leandro, CA 94577

Abstract

A proof-of-concept experiment (POCE) to demonstrate the performance of a novel recirculating induction accelerator has been completed. The Spiral Line Induction Accelerator employs a unique combination of features (spiral beamline, shielded off-axis gaps, and stellarator focussing fields) which permits efficient, high-current operation with a compact device.[1] Initial experiments demonstrated acceleration of 2 and 10 kA beams to 5.5 MeV and acceleration of a 12.5 kA beam to 4.5 MeV by transport around a full turn with two passes through a single accelerating unit. Recent tests with the completed POCE hardware achieved the program goal with acceleration of a 2.4 kA beam to 9.5 MeV.

1 INTRODUCTION

The Spiral Line Induction Accelerator (SLIA) is a compact high-current accelerator with two accelerating units placed on each side of a racetrack geometry (Fig. 1). An electron beam is recirculated through the accelerating units using a spiral beamline for simple injection and extraction. A solenoidal magnetic field confines the beam in the accelerating units; and toroidal, vertical, and stellarator fields are used for transport through the bends. The $l = 2$ stellarator or helical quadrupole fields [2] permit transport of a high current beam with large energy spread (design goal: transport of injected beam with $\leq 20\%$ energy spread), and a shielded gap design permits off-axis accelerating gaps which are necessary for the spiral line geometry. This report describes a SLIA POCE experiment which consists of circulation around three 180° bends with two passes through each of the two

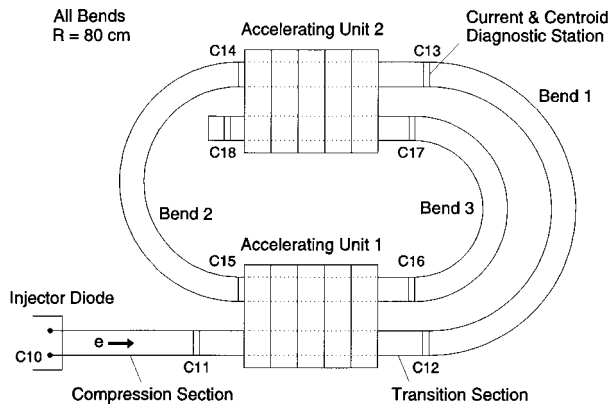


Figure 1. SLIA layout and diagnostic stations.

accelerating units.

Major issues pertinent to SLIA operation are: (1) transport efficiency, (2) energy bandwidth of small aperture bends, (3) excitation of transverse beam deflection modes in the cells, i.e. the beam break-up instability (BBU), and (4) beam envelope matching on and off the stellarator bends.

The field-free injector diode uses a velvet cathode in a Pierce field geometry. The energy variation during the current risetime is $\sim 65\%$, and $\sim 100\%$ during the falltime. The compression region consists of six solenoids tuned to provide a field profile which minimizes envelope oscillations for peak and near-peak injected energies. Beam diameter at the compression exit for these experiments is 12 mm. Each accelerating unit has five induction acceleration cavities, and each cavity has two off-axis accelerating gaps. Each gap produces a 300 kV, 83 ns FWHM accelerating pulse. The toroidal field in the accelerating units was ~ 2 kG. Transition sections 56.7 cm long are inserted between the accelerating units and bends 1 and 3. These allow diagnostic access and capability for addition of matching coils if needed.

The three 180° bends all have an 80 cm major radius and a 3 cm beampipe radius. Each bend has three layers of windings as outlined in the table below.

Table 1. Typical field values in the bends.

Toroidal (kG)	Vertical (G)	Stellarator (G/cm)
3.5 - 3.8	221 - 342	87 - 105

The stellarator pitch is 62.8 cm in bend 1, 83.8 cm in bend 2, and 125.7 cm in bend 3. These values allow operation of the bends as first order achromats. No steering or matching coils were used in the experiments reported here although experiments to validate two matching techniques [3] were conducted during the program.

There are nine B-dot stations labeled C10 through C18. Each station has 4 B-dots oriented at 90° intervals. Beam current is determined from addition of the 4 B-dot signals and beam centroid displacement is derived using a ratio equation involving the signals from opposing B-dots. A time integrated camera which images a Cherenkov converter is used to infer beam size. The target for this diagnostic consists of (1) a carbon disk and (2) two quartz plates separated by conducting mesh for

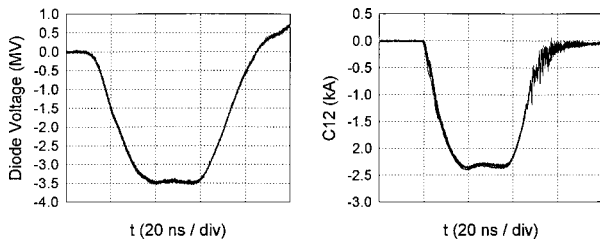


Figure 2. Seven shot overlay of diode voltage and C12 current charge bleed-off.

2 BEAM MEASUREMENTS

Figure 2 shows reproducibility of diode voltage and C12 current for a seven shot overlay. Low energy electrons are not matched to the fields in the compression region and execute large radial oscillations in the compression region and accelerating unit. This produces current occlusions responsible for the oscillations observed during the falltime of the C12 current. In later work insertion of apertures in the compression section eliminated these oscillations. Beam centroid motion during ~ 25 ns of the current pulse at the end of the linear section of the accelerator (C12) was ± 0.3 mm, the limit of resolution of the B-dot array.

Beam current and displacement at C16, C17, and C18 are given in Fig. 3. Beam displacement is shown for current $\geq 80\%$ of the maximum current. The beam

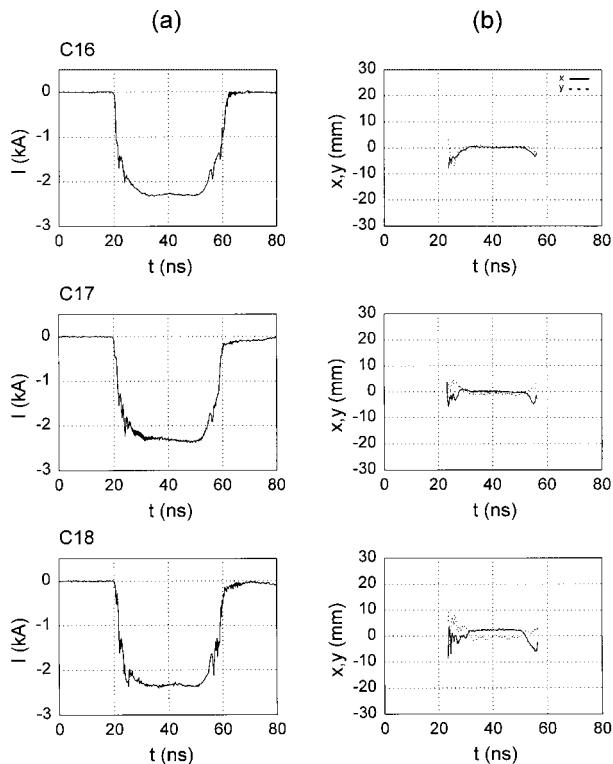


Figure 3. (a) Beam current. (b) Beam displacement. Shot # 4496.

current profile is maintained throughout the transport with minor perturbations. During the mid-pulse at C16 and C17 (entrance and exit of bend 3) both x and y displacements are ≤ 1 mm and vary $\leq \pm 0.5$ mm. During the midpulse at C18 x-displacement is 3 mm and varies $\leq \pm 0.5$ mm, and y-displacement is ≤ 2 mm with oscillations $\sim \pm 1$ mm amplitude. The significantly larger displacements during the pulse rise and fall time are due to large energy mismatch in the bends which results in off-axis, larger angle trajectories at the bend exits.

Figure 4 gives maximum beam current, beam energy, and total beam charge as a function of axial position in

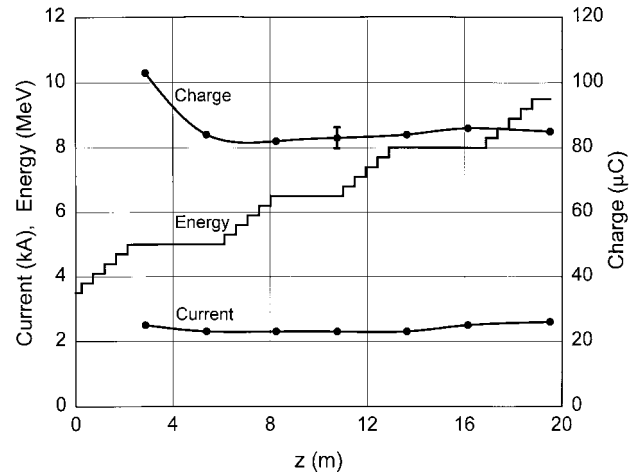


Figure 4. Beam current, energy (kinetic plus potential), and charge vs. beamline location.

the spiral line. The plot begins at the entrance to accelerating unit 1. The data points on the current and charge plots correspond to B-dot stations C12 - C18. The energy curve shows acceleration from the injector energy (3.5 MeV) to the final design energy (9.5 MeV). The loss of charge between C12 and C13 is due to loss of lower energy electrons in the risetime and falltime which are below the energy acceptance of bend 1. There is no additional loss of charge from C13 to C18. The small fluctuations are within the $\pm 3\%$ accuracy of the measurement. The maximum current level is maintained throughout the spiral line.

The total system energy bandwidth is determined by comparison of the transported current and the diode voltage (Fig. 5.) The transported current pulse measured at C18 is identical to the injected current (C10) except the leading and falling edges are truncated as shown by the vertical lines in Fig. 5. Electrons which are $\geq 80\%$ of the peak injected energy are transported through the entire spiral line; therefore the system energy bandwidth is 20%.

A time-integrated measurement of beam profile recorded immediately downstream of C18 is given in Fig. 6. The black outer boundary is the 60 mm beampipe

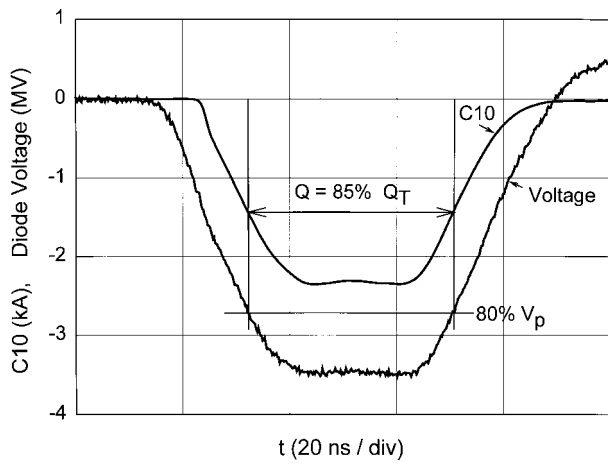


Figure 5. Determination of system energy bandwidth.

diameter. The full-width half maximum (FWHM) of the Cherenkov light is 18.6 mm. Calibration of light output with current density is required to rigorously determine beam width from this measurement. Previous work at lower beam voltage has demonstrated good agreement between light output and beam size.[4]

The two main modes of BBU growth are 1.0 and 1.8 Ghz from RF cold tests of a prototype cell/cavity.[5] Excitation frequencies below 900 MHz do not couple through the coaxial section of the shielded gaps. No evidence of BBU growth was observed in any of the SLIA experiments even though no Q-reduction ferrite pieces were incorporated in the cells. Asymptotic formulas suggest BBU gains as high as ~ 230 for the 1.0 Ghz mode with some experimental parameters.

Stellarator fields are used to increase energy bandwidth in the bends. If stellarator fields are turned off energy bandwidth is reduced. Current rise and fall times

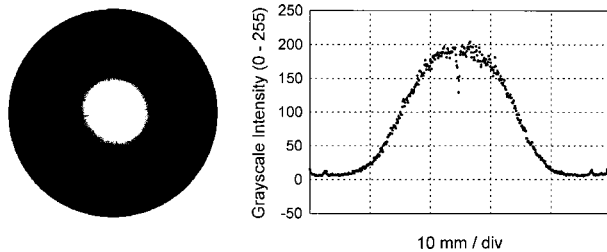


Figure 6. Cherenkov image of electron beam at the accelerator exit, and a line scan across a diameter. Cherenkov diameter = 18.6 mm, x-displacement = 0.6 mm, y-displacement = 0.6 mm. Shot # 4306.

which consist of lower energy electrons are significantly affected by the reduced bandwidth. This is demonstrated by comparison of risetime and falltime features at C18 for two cases: (1) all bends had stellarator fields - Fig. 3, and (2) only bend 3 had a stellarator field - Fig. 7.

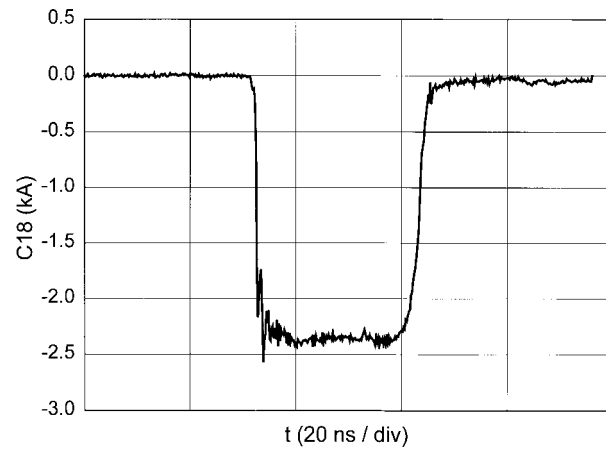


Figure 7. Current at C18 for shot without bend 1 and bend 2 stellarator fields. Risetime = 0.6 ns, FWHM = 31 ns. Shot # 4502.

3 SUMMARY

The SLIA proof-of-concept experiment has demonstrated acceleration of the 2.4 kA beam with an initial energy spread of 20% to full design energy. There was no measurable loss of charge after the first bend which eliminated electrons with energy outside the design energy bandwidth. At the accelerator exit the indicated beam diameter was 18.6 mm, and transverse centroid oscillations during the midpulse were less than $\sim \pm 1$ mm. Shot-to-shot reproducibility of current profiles and spot size were excellent. No oscillations due to BBU were observed, and no matching or additional steering were required for efficient transport.

4 ACKNOWLEDGMENTS

The excellent technical work by John Lisherness of Pulse Sciences, Inc. and the support of William Freeman of the Naval Surface Warfare Center and Dr. Bertram Hui of the Defense Advanced Research Projects Agency are very much appreciated. Theoretical support by the Naval Research Laboratory and Science Applications International (McLean, VA) during the early phase of the program and by Mission Research Corporation (Albuquerque, NM) throughout the program is gratefully acknowledged. This work was sponsored by DARPA and monitored by NSWC.

REFERENCES

- [1] S. D. Putnam, 1987 IEEE Particle Accelerator Conference, Conf. Record 87CH2387-9, p. 887. V. Bailey et al., *ibid.*
- [2] C. Roberson et al., *Particle Accel.* **17**, p. 79 (1985).
- [3] M. Tiefenback et al., 1991 IEEE Particle Accelerator Conference, Conf. Record 91CH3038-7, p. 3195; J. Krall et al., *J. Appl. Phys.* **77**, p. 463 (1995).
- [4] J. P. Lidestri et al., 1991 Particle Accelerator Conference, Conf. Record 91CH3038-7, p. 3120.
- [5] J. Edighoffer, 1991 IEEE Particle Accelerator Conference, Conf. Record 91CH3038-7, p. 3117.